Eur. Phys. J. D **37**, 93–103 (2006)
DOI: 10.1140/epjd/e2005-00245-y

THE EUROPEAN PHYSICAL JOURNAL D

The structuring of a molecular dopant in a quantum solvent

$OCS(H_2)_N$ Van der Waals clusters

C. Piccarreta[a] and F.A. Gianturco[b]

Department of Chemistry and INFM, University of Rome, La Sapienza, Piazzale A. Moro 5, 00185 Rome, Italy

Received 20 June 2005 / Received in final form 11 July 2005
Published online 30 August 2005 –

Abstract. The structural features of a varying number of pH_2 molecules bound to one dopant molecule of OCS are examined using quantum calculations with the Diffusion Monte Carlo (DMC) approach. The interaction forces were obtained from ab initio calculations for the OCS–pH_2 system and for the pH_2 dimer. The overall potential energy surface is then constructed as a sum of interpartner potentials where the pH_2 molecules are treated as spherical species. The calculations suggest that pH_2 molecules indeed behave as a quantum solvent and that an initial "doughnut" of five to six equivalent pH_2 partners is formed on the bisecting middle plane perpendicular to the OCS main axis, showing there strong spatial delocalization. Further added molecules move sequentially to either end of the dopant species, a process seen here to be increasingly more affected by the H_2–H_2 interactions contributing to clusters stability.

PACS. 34.20.-b Interatomic and intermolecular potentials and forces, potential energy surfaces for collisions – 34.20.Gj Intermolecular and atom-molecule potentials and forces

1 Introduction

The increasing use of liquid ^{4}He and ^{3}He droplets as a unique environment for molecular systems has been shown in recent years to have opened up many opportunities for very precise and highly resolved molecular spectral line measurements and for probing superfluid phenomena at the atomic scale in a finite system [1–3]. The excellent agreement of the observed spectra with simulations based on model Hamiltonians for the free molecules suggested that the dopant molecules rotate almost freely within the droplet [3] and the comparison of, say, the spectra found for OCS in ^{4}He with those in ^{3}He was used to connect the above phenomenon with the superfluid nature of the bosonic helium droplets [4–6].

Recent experimental efforts [7–9] have further taken up the analysis of composite clusters surrounding the dopant OCS molecule by attempting to study the structure of a fairly simple Van der Waals (vdW) complex formed inside a ^{4}He droplet or in mixed ^{4}He/^{3}He droplets. In particular, the rotational spectra of OCS with para-H_2, HD and ortho-D_2 molecules inside a cold (0.15 K) mixture of helium atoms have been used to determine the structure of the complexes with a variable number of H_2 molecules [10]. In those studies, among other things, the authors discovered that the infrared (IR) spectra of $OCS(H_2)_n$ clusters which are rotating in cold (0.15 K) superfluid ^{4}He droplets coated with ^{3}He, exhibit resolved rotational bands which are well separated for each n, up to $n = 8$ indistinguishable para-H_2(pH_2) or distinguishable ortho-D_2(oD_2) molecules. Their analysis of the spectra further suggested that the H_2(D_2) molecules form rings around the linear OCS chromophore and that the overall VdW complex behaves like a free asymmetric top defined by three rotational constants. The moments of inertia of these complexes were further found to be a factor of 3 to 10 larger than those estimated for the free complexes. In the larger aggregates it was surmised from the experiments [9,10] that the He atoms from the bath are replaced one-by-one by the hydrogen or deuterium molecules which are similar in size to He atoms but are instead *distinguishable* from both the atoms of the droplet. The further difference between using either pH_2 or oD_2 was also found to have a profound effect on the spectral structures in the superfluid droplets [9–11].

Since the interaction between the H_2 molecule and the OCS dopant is much stronger than that of both the above partners with He, we felt that one possible first step for understanding the above experimental behaviour from first principles was to look at the structures of the clusters where the pH_2 molecules alone are used as an environment for the OCS molecule and to observe the changes occurring as their number is being increased to span the range of values employed in the experiments. The additional effects of adding ^{4}He atoms to the cluster in order to also model the behaviour of the experimental droplets that contained

[a] :*Present address*: Dept. of Physics and Astronomy, University College London, Gower Street, London, UK.
[b] e-mail: fa.gianturco@caspur.it

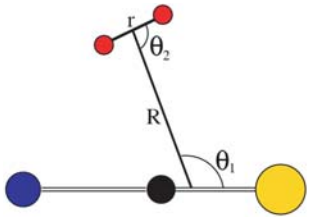

Fig. 1. Geometry of the internal coordinates system in OCS–(H_2) complex. The sulphur atom is on the left and the dihedral angle φ (not shown) is the angle between the planes defined by the OCS-axis and the R coordinate and by the H_2-axis and the same R coordinate.

the VdW OCS$(H_2)_n$ complexes will be dealt with in future work. Here we limit ourselves to the detailed analysis of the possible structures of the aggregates that contain various pH_2 molecules attached to the OCS dopant.

Earlier theoretical work on the present system [12,13] has also analysed the relative structuring of the pH_2 as structureless particles around the OCS molecule and has limited the study to the smaller clusters. We shall therefore expand the study to larger OCS$(pH_2)_n$ aggregates with n up to 30.

2 The intermolecular potentials

2.1 The averaged energy surfaces for OCS-pH_2

The geometry of the complex we are studying is given in its simplest form by only one pH_2 molecule added to OCS. In Figure 1 we report the Jacobi coordinates between the two centers of mass (R, ϑ_1) and the orientational coordinates (φ, ϑ_2) for the attached H_2 partner. The angle φ defines the dihedral angle between the two planes with contain (R, OCS) and (R, H_2) respectively. The internuclear distances are kept in OCS at its equilibrium values of $r_{O-C} = 2.151$ a.u. and $r_{C-S} = 2.943$ a.u., while for H_2 the vibrationally averaged value (1.449 a.u.) was used. The presence of vibrationally excited molecular partners is not considered in the present study and we therefore treat both partners as rigid rotors (RR's).

The full interaction potential, given as a function of $(R, \vartheta_1, \vartheta_2, \varphi)$, has recently been computed [14], using Dunning's aug-CC-pVTZ basis plus additional bond functions, and with correlation corrections at the MP4 level [14]. The radial range between partners was considered to vary from 2.5 to 8 Å while the ϑ_1 values ranged from 0° to 180° in 15° intervals. For each set of the above Jacobi coordinates the orientation angle ϑ_2 took three values and the dihedral angle φ took also three values. The possible different orientations of the (φ, ϑ_2) couplets for the pH_2 partner available from the calculations were: (0°, 0°), (0°, 90°) and (90°, 90°).

We have employed the raw points computed by reference [14] to generate a model potential energy surface (PES) where the pH_2 molecule is being treated as a spherical partner in its $j = 0$ state, a simplification also employed in the earlier interpretations of the experimental

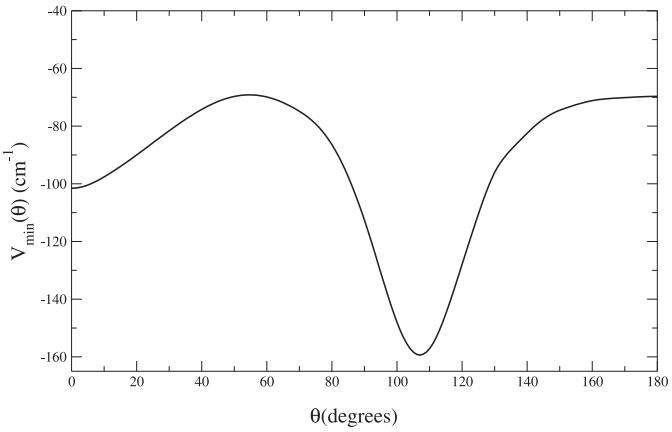

Fig. 2. Minimum energy angular profiles computed for the two PES employed in the present work.

data [7–10] and also by the more recent calculations [12, 13]. The latter, averaged Potential Energy Surface (PES) is now a function of two variables only and was in turn expanded into spherical harmonics to obtain a smooth and accurate representation of the interaction over the whole space spanned by the original raw points of the Potential Energy Surface (PES) [14]. We shall call it the $V_{av}(R, \vartheta)$ potential, with the latter angle θ being the one labelled as ϑ_1 in Figure 1. The physical picture behind this choice is that of a free rotating complex of OCS...H_2 with the hydrogen molecule treated as a non rotating partner. It is interesting to note that, when the V_{av} potential is employed to obtain the rotational constants for the complex, we found them to be (in cm^{-1}): $A = 0.7556$, $B = 0.1994$ and $C = 0.1541$. Such data, for $J = 0$, turn out to be in rather good accord with the measurements by Mc Kellar and coworkers [15]: $A = 0.7607$, $B = 0.1999$ and $C = 0.1534$. The corresponding measurements by Grebenev et al. [10] were: $A = 0.699$, $B = 0.197$, $C = 0.151$, again rather close to the above computed values. The same averaged Potential Energy surface has been used recently [13] to evaluate the rotational structures and energetics of OCS$(H_2)_n$ with n up to 8 and turns out to be entirely identical to ours.

The plot of Figure 2 show the general anisotropy of the averaged PES: we report there the angular minimum energy paths (AMEP), $V_{min}(\vartheta)$, as a function of ϑ. One clearly sees there that three different "well" regions appear around the OCS molecule, with the central one around 100° being the strongest attractive region of the present potential. The local and global minima are: at 0° with -91.4 cm^{-1}, at 105° with -144.6 cm^{-1} and at 180° with -69.2 cm^{-1}. They are also the same as those obtained by reference [13].

2.2 The bound states of the complex

In order to determine the structures of the bound wavefunctions supported by the smallest VdW complex with a single pH_2 attached to the dopant, we employed our V_{av} potential and used both the collocation method, as implemented by Cohen and Saykally [16,17] and the

Table 1. Computed binding energies of the OCS(pH_2) complex using the two different PES discussed in the main text and two different methods of calculation. All values in cm^{-1}. Results are for the $J = 0$ case.

	Collocation [16, 17]	Bound [18]
n	$V_{av}(cm^{-1})$	$V_{av}(cm^{-1})$
0	−77.375995	−77.944292
1	−46.990777	−46.891814
2	−46.440260	−46.346374
3	−33.706509	−33.853747
4	−29.476013	−29.543187
5	−24.540732	−24.591004
6	−19.538897	−19.694052

close-coupling calculations within the BOUND suite of programs [18]. For the former calculations we employed 33 radial functions (Morse functions) and 30 angular functions (Legendre Polynomials) and reached a numerical stability of around 2%, while for the latter method we achieved a numerical stability of 10^{-3}. The first seven states are listed in Table 1 for the $J = 0$ VdW complex; we see only qualitative agreement between the two methods, a level of agreement that we however deem to be sufficient for the present purpose. One can readily make the following comments:

1. the 1st and 2nd excited states given by the PES are very close to one another ($\Delta E_{12} \sim 0.5$ cm^{-1}). This small difference will be an important feature during our following discussion of the cluster's structuring;
2. the higher levels up to $n = 6$ are again well spaced and provide a sequence of H_2 locations within the cluster, as we shall discuss below.

In order to gain a better physical understanding of the spatial positions of such bound states of the complex, we show in Figures 3 and 4, for the first six of them, the radial and angular shapes of the densities of their computed wavefunctions. We show only the results obtained with the Collocation Method [16,17]. We can make the following considerations:

1. the lowest bound pH_2 molecule (treated as a structureless sphere) is located at about 3.5 Å away from the OCS main axis and at an angle close to 105°, exhibiting marked delocalization in both coordinates;
2. the V_{av} shows the H_2 molecule in the $n = 1$ level (nearly degenerate with the $n = 2$) to be located further out than that in the $n = 2$ and to be closer to the sulphur atom ($\vartheta^{max} \sim 10°$) while the molecule in the $n = 2$ level is instead closer to the oxygen atom ($\vartheta^{max} \sim 120°$). In other words, the $n = 2$ bound state describes a sort of "bending" excitation of the complex with the pH_2 partner strongly oscillating between the two ends of the OCS molecule;
3. from $n = 3$ and up to $n = 6$, however, the bound states are radially located at similar distances and exhibit rather diffuse angular structures: only the levels up to $n = 5$ are shown in the figures, as we will need them for our following discussion on the larger clusters.

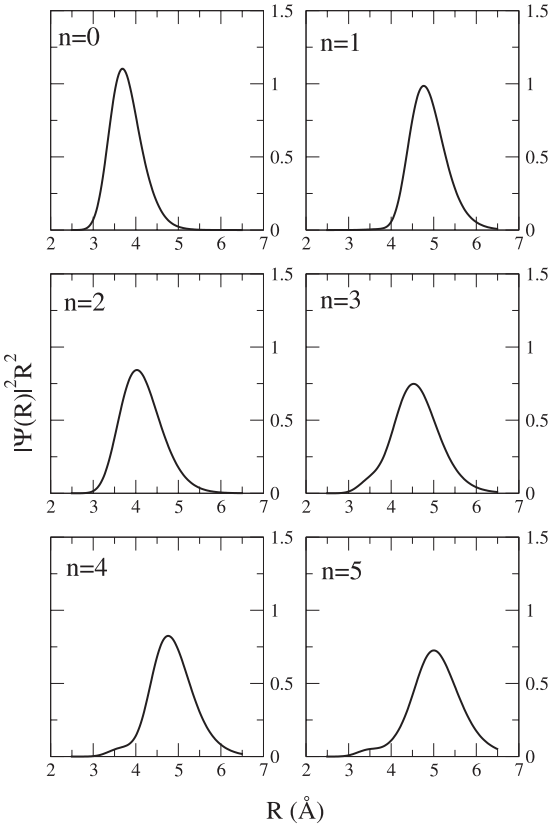

Fig. 3. Spatial shapes of the computed bound states for the OCS(pH_2) complex using both PES discussed in the present work. The six panels of the figure show the radial densities profiles.

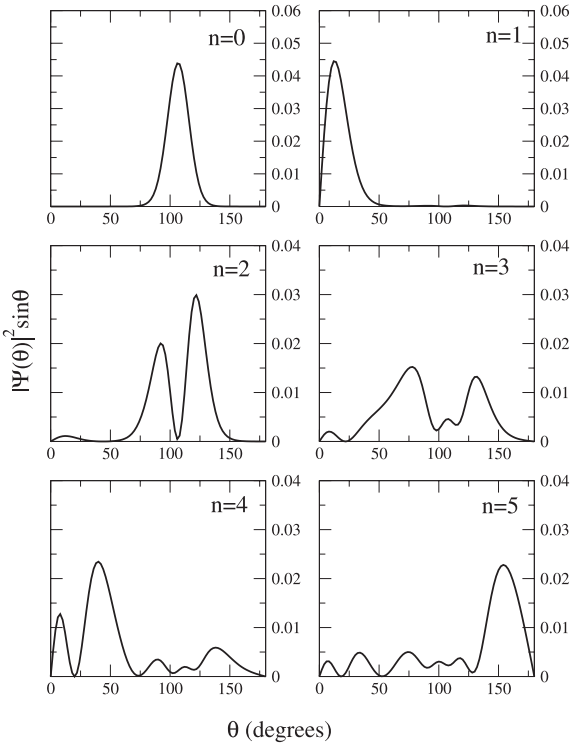

Fig. 4. Same as in Figure 3 but for the angular wavefunction behaviours.

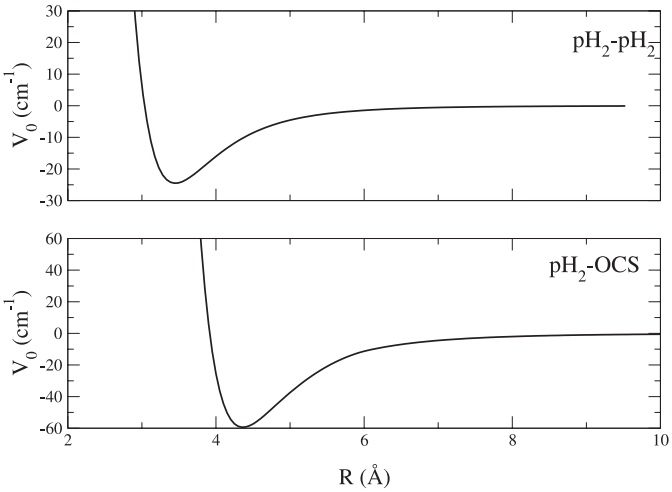

Fig. 5. Computed spherical averaged potential curves for the pH_2–pH_2 system (upper panel) and the OCS–pH_2 system in the lower panel.

2.3 The global interaction within aggregates

To extend our study to larger clusters we now need to look at the differences in strength between the OCS interaction with one pH_2 molecule and the interaction among two pH_2 molecules. The latter quantity has been computed a while ago [19] to obtain the full PES over both vibrational and rotational degrees of freedom and its corresponding multipolar expansion coefficients. The computed PES we are using here has been given in reference [19] and turns out to be slightly different from the best recommended empirical potential suggested earlier on by Buck et al. [20]. In Figure 5 we compare the spherical component (upper panel) of the pH_2–pH_2 interaction given in that work [19] with the same component for the pH_2–OCS interaction: we clearly see that the averaged strength of the potential between the two pH_2 particles is less than that of the solvent molecule with the OCS dopant, a feature which could help us to model the overall potential for the larger aggregates by simply taking it as a sum of two-body potentials, the first of them being the anisotropic OCS–pH_2 PES of the present work:

$$V\left[\mathrm{OCS}(\mathrm{pH_2})_n\right] \simeq \sum_{i=1}^{n} V_{\mathrm{OCS-pH_2}}(R_i,\vartheta_i) + \sum_{j<k}^{n} V^{(0)}_{\mathrm{pH_2-pH_2}}(R_{ik}) \qquad (1)$$

where we disregard possible higher-order, many-body effects due to the interactions between the additional pH_2 molecules around the OCS dopant and also to interactions between several pH_2 partners. Furthermore, we are not considering the orientational features of the pH_2 molecule both in the H_2–H_2 potential and in its interaction with the OCS impurity. It is difficult to gauge at this point the importance of such simplifications, although we shall see that our results seem to indicate that we are already getting the main physics of the solvation process in line with the experimental suggestions.

We will therefore test below the reliability of the above global, simplified PES by carrying out stochastic calculations of the ground state bound structures for a broad number of pH_2 molecules added to the OCS dopant taken as "solvated" within the pH_2 cluster we are constructing around it.

The method of choice, the diffusion Monte Carlo (DMC) method, and its implementation in our present study will be briefly outlined in the next section.

3 The diffusion Monte Carlo method

The diffusion Monte Carlo (DMC) method has been already extensively discussed by us and by others in a number of recent articles [6,21–27]. We thus refer the reader to that literature for a fuller discussion, while this section merely summarises the main features of our treatment and some specific aspects of it.

The key idea of the DMC method is the isomorphism between the solution of the time-dependent many-body Schrödinger equation and a multidimensional reaction-diffusion equation with anisotropic diffusion coefficients. Introduction of imaginary time $\tau = it/\hbar$, shifting of the absolute energy scale by a quantity E_{ref}, and identification of the inverse mass terms with diffusion coefficients D_j and of the shifted potential $[V(\mathbf{r})-E_{ref}]$ with position-dependent rate terms $K(\mathbf{r})$ leads to the following equations which show this analogy

$$i\hbar\frac{\partial\Psi(\mathbf{r},t)}{\partial t} = -\sum_j \frac{\hbar^2}{2m_j}\nabla_j^2\Psi(\mathbf{r},t) + [V(\mathbf{r}) - E_{ref}]\Psi(\mathbf{r},t) \qquad (2)$$

$$\frac{\partial\Psi(\mathbf{r},\tau)}{\partial \tau} = -\sum_j \frac{\hbar^2}{2m_j}\nabla_j^2\Psi(\mathbf{r},\tau) + [V(\mathbf{r}) - E_{ref}]\Psi(\mathbf{r},\tau) \qquad (3)$$

$$\frac{\partial C(\mathbf{r},t)}{\partial t} = -\sum_j D_j\nabla_j^2 C(\mathbf{r},t) + K(\mathbf{r})C(\mathbf{r},t). \qquad (4)$$

Some knowledge of the structure of the wavefunction can be further exploited to increase the accuracy of the final result by introducing a guiding function Ψ_T which approximates the true wavefunction one is looking for. The introduction of Ψ_T results in additional drift terms in the diffusion equations which then direct the random walkers into regions where the trial wavefunction is large. At the same time, the rate terms are now controlled by the local energy defined as

$$E_{local}(\mathbf{r}) = \Psi_T^{-1}(\mathbf{r})\hat{H}\Psi_T(\mathbf{r}) = \Psi_T^{-1}(\mathbf{r})\hat{T}\Psi_T(\mathbf{r}) + V(\mathbf{r}) \qquad (5)$$

which is a smoother function of the coordinates than the potential and reduces the variance of the energy estimators [28]. One can then further rewrite the time-dependent

equation as follows

$$\frac{\partial(\Psi\Psi_T)}{\partial\tau} = \left[\sum_j \frac{1}{2m_j}\nabla_j^2(\Psi\Psi_T) - \frac{1}{m_j}\nabla_j(\Psi\Psi_T\nabla ln\Psi_T)\right] - [\Psi_T^{-1}T\Psi_T + V(\mathbf{r}) - E_{ref}](\Psi\Psi_T). \quad (6)$$

A random walk technique is used to calculate the steady-state solution of (6) and therefore a large ensemble of random walkers is propagated with time steps $\Delta\tau$ starting from some arbitrary initial distribution. We use a Metropolis type acceptance check for each attempted move [22,24–26] such that for arbitrary time steps the number density of walkers is given by Ψ_T^2 in the limit of zero branching, while their weights are a stochastic sample of the local value of Ψ/Ψ_T.

After equilibration of the initial random walker distribution one expects that the ensemble average of E_{local}, which will be the E_{mean}, is identical with the ground state energy irrespective of Ψ_T and is only subject to statistical fluctuations. The ground state energy can also be computed from the rate at which the total weight of the ensemble grows or decays as τ elapses. This estimator is called the growth energy [26,27] of the system

$$E_{growth} = E_{ref} - \frac{\partial lnW(\tau)}{\partial\tau}. \quad (7)$$

A local property expectation value $\langle\hat{A}\rangle$ is obtained by replacing integrals by sums over samples

$$\langle\hat{A}\rangle = \frac{\int \Psi^*(\mathbf{x})\hat{A}\Psi(\mathbf{x})d\mathbf{x}}{\int \mid \Psi(\mathbf{x}) \mid^2 d\mathbf{x}} \quad (8)$$

$$\approx \frac{1}{N_{\mathrm{H}_2}}\sum_{i=1}^{N}\Psi^{-1}(\mathbf{x}_i)\hat{A}\Psi(\mathbf{x}_i). \quad (9)$$

Local operators are directly accessible with the DMC scheme and the integration reduces to an average over $A(\mathbf{x})$ values

$$\langle\hat{A}\rangle \approx \frac{\sum_i^N w_i A(\mathbf{x}_i)}{\sum_i^N w_i}. \quad (10)$$

This technique is in particular applicable to the positional correlation functions which are very useful to visualize the structure of the clusters, as we shall further show below. The radial distribution of the pH_2 "spherical" molecules with respect to the center of mass (c.o.m.) of a given cluster is computed as

$$P_{rad}(R) = \frac{1}{n}\sum_i^{N_{\mathrm{H}_2}}\left\langle\frac{\delta(R_i - R)}{R^2}\right\rangle_{walk} \quad (11)$$

a quantity which can be easily converted to the spherically averaged radial pH_2 density distribution $\rho(R)$

$$\rho(R) = \frac{N_{H_2}}{4\pi}P_{rad}(R). \quad (12)$$

In a similar way we compute two-dimensional histograms in cylindrical coordinates to analyse the density distribution $\rho(r,z)$ of a varying number of pH_2 solvent molecules around the OCS. The later molecular bond is chosen at the z-axis and the perpendicular distance of the pH_2 "spheres" to this axis defines the polar radius r. The origin coincides with the c.o.m. of OCS and the oxygen atom is on the negative z-axis. The density distribution is therefore obtained as

$$\rho(r,z) = \frac{N_{\mathrm{H}_2}}{2\pi}\sum_i\left\langle\frac{\delta(r_i - r)}{r}\delta(z_i - z)\right\rangle_{walk} \quad (13)$$

where

$$N_{\mathrm{H}_2} = 2\pi\int_0^\infty\int_{-\infty}^\infty(\rho(r,z)rdrdz. \quad (14)$$

This quantity is accumulated on a grid which is equidistant in z and r^2 and it eliminates the need to take square roots during the data collection.

All calculations were done over a broad range of cluster sizes, using the pairwise additive potential energy surface as discussed before, treating the OCS dopant as a rigid rotor impurity within each pH_2 cluster [29]. The rigid body rotation of the OCS molecule is implemented using the algorithm fully described by [30]. Our present approach is also further described by reference [6]. The initial trial function was chosen by fitting the OCS–pH_2 wavefunction obtained from the previous calculations to a Jastrow form [26] and the corresponding parameters were modified for each N_{H_2} value considered. The actual parameters for the trial functions could be obtained on request from the authors.

4 Results and discussion

4.1 The pH_2 distributions in the ground state cluster

For the $OCS(pH_2)_N$ system with varying number of added pH_2 partners we have analyzed the structures of the ground state wavefunctions for the smaller aggregates with N_{H_2} going from 1 up to 30. The overall number of replicas was first divided into 100 different blocks and the number of walkers per block was between 1000 and 2000. For a cluster of N_{H_2} structureless partners with one OCS molecule described as a rigid rotor, the total dimensionality of the configuration space spanned by the intermolecular vector $\mathbf{R}$ should be $3(N+1)+2 = 3N+5$. Two of these dimensions will refer to the rotational motion, the remainder being for the translational motion of all the constituents.

As already tested in our previous study of $OCS(He)_N$ clusters [5,6], the above dimensionality was attained in two steps. First one samples the translational Green's function for a $3N+6$ dimensional cluster, where the OCS molecule is represented as a pseudodiatom, and then one imposes the rigid rotor constraints on the latter dopant pseudodiatom.

The energy estimators were collected over the blocks of variable size mentioned before and their dependence on

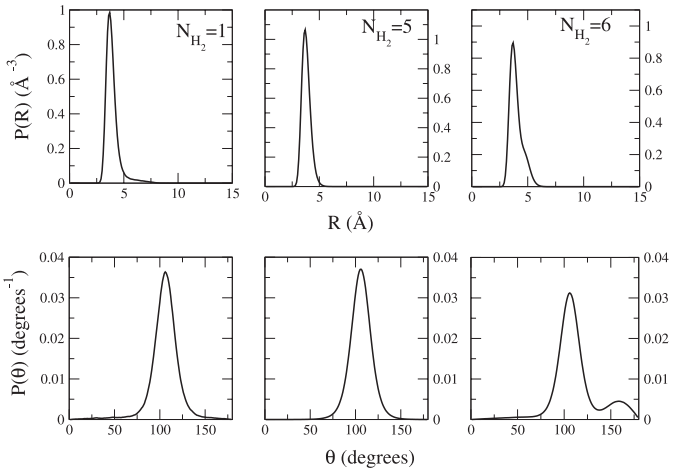

Fig. 6. Computed spatial densities for the bound states of the $OCS(pH_2)_N$ clusters for different members of added molecules. The panels on the top report the radial densities for the wavefunctions with $N_{H_2} = 1$, 5 and 6 normalized to unity, while the panels at the bottom report, with the same notation, the angular densities, also normalized to unity.

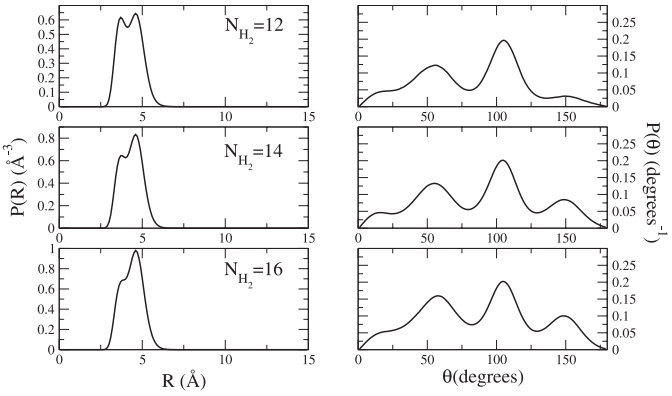

Fig. 7. Same as in Figure 6, but for clusters containing from 12 to 16 pH_2 molecules. The panels on the left show angular densities.

the choice of the time step value $\Delta\tau$ was carefully checked in order to eliminate any significant time step bias. Thus, we found an optimal value of $\Delta\tau = 5$ a.u. and several thousand time steps were employed in order to equilibrate the initial random distribution. The final energy values were analysed also in relation to their dispersion values. The latter went from less than 1 cm^{-1} for the smaller clusters to a maximum of $\sim$5 cm^{-1} for the largest aggregates we examined in the present work ($N_{H_2} = 30$).

To assess the quality of our ground state wavefunction for the $OCS(pH_2)$ complex, we compared the angular distributions of $|\Psi_0|^2$ using both the DMC algorithm and the collocation method discussed before. We found that both methods provide very similar shapes for the two bound states, with their binding energies agreeing within less than 1%. We therefore employed the collocation results as a trial function for our larger clusters, having assessed the closeness of the DMC data with those from the collocation algorithm [17].

In Figures 6 we report the radial and angular densities, respectively, for the $OCS(pH_2)$ clusters with N_{H_2} going from 1 to 6. The computational results were obtained using both the PES discussed earlier for the V_{OCS-H_2}, while the $V_{H_2-H_2}$ interaction is always taken to be the spherical component of the full PES from reference [19] The following comments could be made:

1. the first five pH_2 additional partners show very similar radial density shapes, peaking at about 3.6 Å from the center of mass and forming at the peaks an angle of $\sim$107° with the dopant molecular axis, i.e. slightly above the mid-bond location and more towards the oxygen atom. One could thus qualitatively say that the first five atoms are strongly equivalent partners, are also highly delocalized (radially and angularly) and resemble the shape of a "doughnut" around the dopant OCS [9,10];
2. on the other hand, part of the sixth atom gets located further away from the molecular axis, closer to $\sim$4.8 Å, and forms a larger angle with the z-axis, getting closer to the oxygen atom of the OCS molecule.

The spatial picture which emerges from the smaller clusters with up to 6 pH_2 partners indicates that all of them are essentially equivalent and are producing delocalized distributions which are strongly reminiscent of the one-partner ground state w.f. of the OCS (pH_2) discussed before (see Figs. 3 and 4). Hence, one may argue that, at least in the smaller clusters, the pH_2 interaction with the dopant molecule largely controls the cluster shapes, while the $V_{H_2-H_2}$ potential acts chiefly as a perturbation within the total interaction. The first few partners thus essentially occupy nearly independent, $n = 0$ states of the one-pH_2 complex. The presence of further pH_2 molecules, however, could be seen to cause additional contributions from the $n = 1$ level (see Figs. 3 and 4) of the single "particle" complex $OCS(pH_2)$, since the ϑ Jacobi angle angle is now more strongly tilted towards the O atom. The near-degeneracy between the $n = 1$ and $n = 2$ states seems to favour the occupancy of the latter which thus produces the angular shape of the $N_{H_2} = 6$ cluster density that shows contributions from larger ϑ values.

One could therefore qualitatively picture the results from the DMC calculations for the larger clusters in terms of the effects on the final energies due to the increasing importance of the "excited" states of the monomer complex in describing the final configuration of the cluster, where the simple picture of independent particle, Hartree-type, monomer "orbitals" in their ground states becomes modified by the contributions of such "excited" single-particle states.

Some of the larger cluster structures up to $N_{H_2} = 16$ are given in Figure 7. It is interesting to note that the radial distributions maintain a sort of two-peak structure, thus qualitatively suggesting the participation of both the ground and first two excited states of the single-pH_2 "orbitals" in describing the total wavefunctions of the different aggregates around the OCS. They show that the first six added pH_2's get chiefly located on the "doughnut"

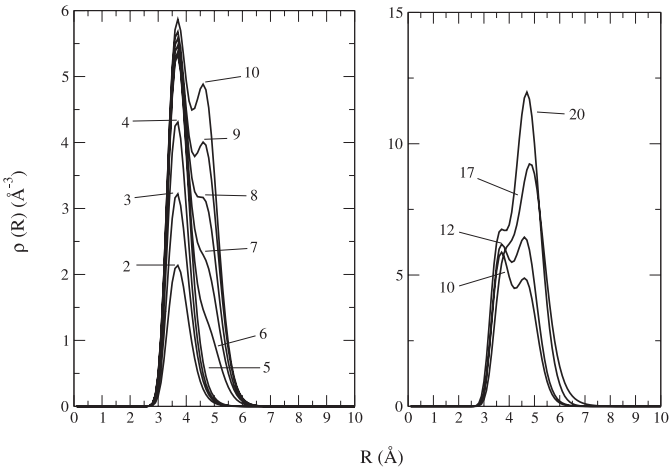

Fig. 8. Computed radial density distributions using the V_{av} potential energy surface. Left panel: for a number of pH_2 solvent molecules from 2 to 10. Right panel: same computed densities for clusters with $N_{H_2} = 10$ and up to 20.

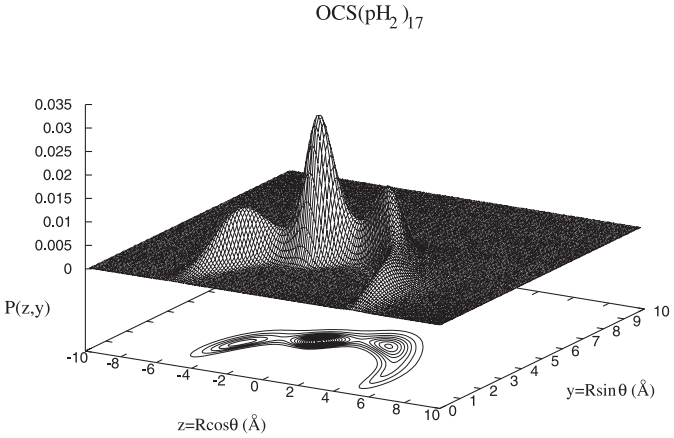

Fig. 9. Computed pH_2 densities surrounding the OCS dopant molecule, locating along the z-axis, with the oxygen atom on the negative axis. The number of particles in the various regions are (from left to right): 4, 6, 6 and 1.

configuration (the $n = 0$ level of OCS–pH_2) then the additional partners preferentially occupy the sulphur and the oxygen sides of the dopant as seen in the $n = 1$ and $n = 2$ levels of the monomer complex in Figure 4 and shown by the right-side panel of Figure 7.

A global description of the results discussed thus far could be gleaned by examining the radial density distributions reported in Figure 8. All quantities are normalized to the total number of pH_2 partners in each cluster.

The left panels show the case of the smaller clusters with N_{H_2} varying from 2 to 10. We clearly see there that the first six pH_2 occupy essentially equivalent positions, all spatially delocalized with peaks around 3.7 Å. In the larger aggregates we see that the next group of added pH_2 partners, up to the $N_{H_2} = 10$ cluster, increasingly populate the second region around the dopant molecule, creating a marked additional layer of pH_2 molecules which peak around 5 Å. The analysis of their angular distributions further suggests that these partner molecules populate a region that is chiefly located on the side the sulphur atom and further cause the sixth partner to get back within the previous ring-like region, moving away from the oxygen-end of the OCS. These findings appear to be in agreement with the experimental suggestions on such OCS $(pH_2)_N$ complexes embedded in He clusters [7–10]. The experiments suggest, in fact, that both the C_5 and C_6 symmetry for the rotating complex would lead to a vanishing ratio of the intensities, I_Q/I_R, [9,10] and our calculations suggest that one can have either five or six pH_2 partners populating the "doughnut" ring. Hence, the present results qualitatively show that a sort of five-fold symmetry exists in the cluster with N_{H_2} up to 5, while a near-sixth fold symmetry appears when the sixth pH_2 partner is located near the 0-end of the molecule and close to the OCS main molecular axis. In the larger clusters the sixth fold symmetry should then be restored by forcing the sixth adatom closer to the molecular ring region.

This behaviour could be seen from the spatial density distributions reported, in cylindrical coordinates, by the data of Figure 9 for the OCS$(pH_2)_{17}$ complex. We show there the OCS molecule placed on the z-axis, with the S atom along the positive direction. The locations of the pH_2 molecules appear to be much more orientation-dependent than was the case for OCS$(He)_n$ clusters we discussed elsewhere [6]: one can clearly see four, well marked regions which contain up to four pH_2 molecules on the oxygen side, six of them in the doughnut ring, six again towards the sulphur region and one closer to the axial sulphur area, as we shall further analyse below.

4.2 Selective locations of (pH_2) partner

The angular anisotropy of the potential describing the OCS–pH_2 interaction (see Fig. 2) shows qualitatively the presence of three distinct regions: (i) the small-angle region on the sulphur side where a well with a depth of about 100 cm^{-1}; (ii) the "doughnut" region around the middle of the molecular axis where the strongest interaction and the deepest well exist; and (iii) the region of the larger angles on the oxygen side where the well is the least strong, i.e. around 50–70 cm^{-1}. As we have already shown with our previous analysis of the OCS$(He)_n$ system [5], it is instructive to artificially create different "boxing" areas comprising these regions by evaluating the total densities of pH_2 partners in each cluster only within limited angular sectors. Because of the more marked anisotropy of the OCS–pH_2 interaction in comparison with the one for the OCS–He system, we find that it is more useful to divide the whole angular region into four different sectors of the Jacobi angle ϑ) (see Fig. 1): the axial S region (between 0° and 25°), the S-side region (between 26° and 75°), the doughnut region (between 76° and 120°) and the 0-side region (between 121° and 180°) The results of our numerical experiment are reported by Figure 10 for the four

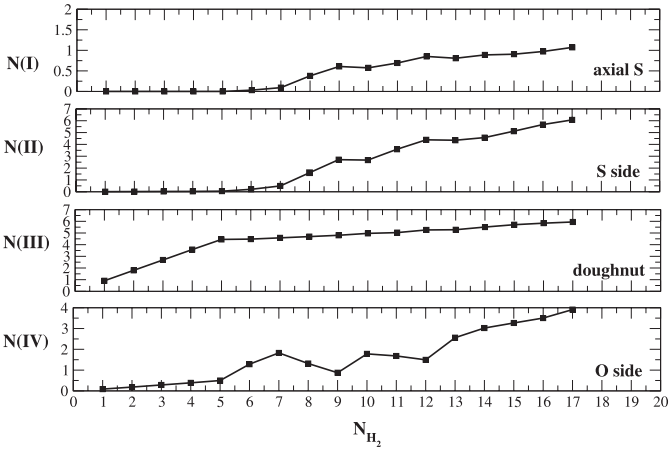

Fig. 10. Density distributions of the pH_2 partners allocated to four different angular sectors, each comprising an angular region of the total PES described in the main text. The distributions are given for the clusters up to 17 pH_2 partners.

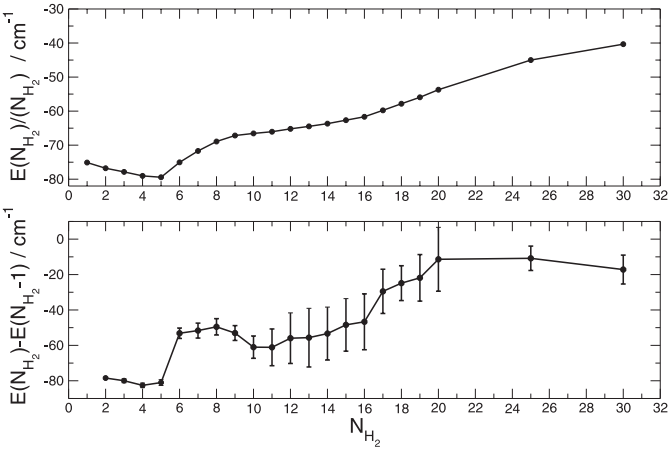

Fig. 11. Upper panel: computed DMC average binding energies for the ground state configurations of the $OCS(pH_2)_N$ clusters as a function of N_{H_2}. Lower panel: computed single-partner evaporative energies for the $OCS(pH_2)_N$ clusters as a function of N_{H_2}. The error bars are shown on the energy differences of the lower panel as compounded errors.

regions described above and for the first 17 admolecules. The following considerations could be made:

1. the region leading to the axial sulphur atom only contains about one pH_2 molecule;
2. the region roughly corresponding to the sulphur side of the dopant molecule is seen not to locate any pH_2 density during the initial addition of six molecules, while it slowly takes on additional pH_2 partners when the cluster size grows from $N_{H_2} = 7$ to 17. We therefore see that during the cluster growth beyond $N_{H_2} = 6$, several pH_2 molecules get localised in the sulphur region which acquires a total density of six pH_2 partners by the time the size of the cluster reaches 17 molecules;
3. the central region of the ring around the molecular axis clearly indicates that *all* the initial five pH_2 partners get located in it. However when two further pH_2 molecules are added to the cluster, the density increment of the central region is only a fraction above $N_{H_2} = 5$ and slowly resumes adding one molecule to that area completing a ring of six molecules by the time the cluster contains 17 partners;
4. the fourth sector, which defines roughly the region around the oxygen end of the OCS, shows a negligible pH_2 density for the first five molecules. The sixth pH_2 molecule gets located in this region of the dopant but is pushed back when more pH_2 partners are added to the cluster, essentially moving to the sulphur side and eventually around the doughnut. However, we clearly see that beyond $N_{H_2} = 12$ the region around the S atom steadily acquires additional density rising up to four pH_2 partners for $N_{H_2} = 17$, confirming what we have discussed earlier about the shape of the distributions given in Figure 9. Thus, the density growth around the oxygen side remains fairly negligible up to $N_{H_2} = 12$, confirming the corresponding preferential allocation of the added pH_2 molecules into the sulphur side of the potential, where the well region is deeper than on the oxygen side (see Fig. 2);
5. beyond the first shell of 12 pH_2 partners, we therefore see a marked increase in the number of particles in the oxygen region, which now acquires 2 pH_2 molecules when $N_{H_2} = 13$, at the expense of the region on the sulphur side. The further increase up to the cluster with 17 molecules shows the presence of about six partners in the oxygen side and the further allocation of molecules at the sulphur side.

In conclusion, our calculations appear to confirm the possibility of a symmetric rotor structure of the clusters up to $N_{H_2} = 5$ to 6 [9,10] and a more complicated filling pattern beyond that size, with the final formation of asymmetric rotor complexes in the larger clusters as surmised by experiments. It is also interesting to notice that when the calculations of the sector distributions was carried out up to $N_{H_2} = 20$, the three additional molecules did not fill the oxygen side but increased instead the pH_2 densities of the two central peaks.

4.3 Energetics of the OCS $(pH_2)_N$ clusters

The structures of the VdW clusters with varying number of bosonic pH_2 are obtained from the wavefunctions associated to the lowest bound, nodeless ground states of the systems. Thus, our DMC calculations directly provide the E_{tot} values, at zero Kelvin, of the clusters we have studied. The behaviour of the average binding energy as a function of N_{H_2} is reported in the upper panel of Figure 11. The actual numerical values are given by Table 2. The following considerations could be made:

1. the total energy for the first five clusters could be obtained reasonably well as a sum of five times the $n = 0$ energy level of the single OCS–pH_2 complex shown in Table 1. For $N_{H_2} = 5$, for instance, the sum gives -387 cm^{-1}: the computed E_{tot} is -397 cm^{-1} for

Table 2. Binding energies from DMC calculations for the $OCS(pH_2)_N$ clusters as a function of N_{H_2}. All values in cm^{-1}.

N_{H_2}	E_{tot}	ΔE_{tot}	E_{tot}/N_{H_2}
1	−75.105		−75.105
2	−153.558	−78.45 ± 0.44	−76.78
3	−233.531	−79.97 ± .1.11	−77.84
4	−316.104	−82.57 ± 1.28	−79.03
5	−397.117	−81.01 ± 1.65	−79.42
6	−450.227	−53.15 ± 2.95	−75.04
7	−501.911	−51.64 ± 4.21	−71.70
8	−551.430	−49.52 ± 4.63	−68.93
9	−604.462	−53.03 ± 4.19	−67.16
10	−665.468	−61.00 ± 6.31	−66.55
11	−726.571	−61.10 ± 10.38	−66.05
12	−782.513	55.94 ± 14.27	−65.21
13	−838.146	−55.63 ± 16.57	−64.47
14	−891.480	−53.33 ± 14.94	−63.68
15	−939.910	−48.43 ± 14.82	−62.66
16	986.587	−46.67 ± 15.78	−61.66
17	−1016.083	−29.50 ± 12.5	−59.77
18	−1040.931	−24.85 ± 9.84	−57.83
19	−1062.797	−21.86 ± 13.14	−55.94
20	−1074.174	−11.38 ± 18.05	−53.71
25	−1124.985	−10.82 ± 6.88	−45.00
30	−1210.018	−17.18 ± 8.16	−40.33

the latter. Thus, the picture of five equivalent partners nearly independently bound to the OCS dopant appears to hold reasonably well for both potential surfaces. This is also in keeping with the picture of an Hartree-like product wavefunction where each single-particle orbital is realistically given by the ground state orbital of the (OCS–pH_2) system, $\varphi_o(\bar{r}_1)$;

2. for the $N_{H_2} = 6$ cluster our analysis of its shape indicates that the additional pH_2 first populates the $n = 1$ level of the $OCS(pH_2)$ complex. Here again the total energy found by our DMC calculations is nearly equal to the sum of the individual energies from the one-partner complex and using the ground state wavefunction of the latter;
3. for the larger clusters up to $N_{H_2} = 12$, the zeroth order scheme still holds remarkably well: the calculations with the V_{av} potential yield a zeroth order structure of -747 cm^{-1} for the configuration (6|3|3) close to its computed DMC E_{tot} value of ~ -782 cm^{-1}. This notation simply describes a cluster with six H_2 partners which all occupy the $n = 0$ level of the OCS–H_2 system, three in the level $n = 1$ and further three in the level $n = 2$, using the energy values discussed before for the smallest complex;
4. when the even larger ($N_{H_2} \geq 12$) clusters are examined, however, the simple zeroth order picture of above becomes less clear as increasingly higher bound states of the $OCS(pH_2)_N$ complex have to be invoked to describe the cluster due to the increasing contributions coming from the $V_{H_2-H_2}$ interaction terms.

The average energy values given in the upper panel of Figure 11 clearly show the slow decrease of the average binding of one H_2 molecule as the cluster grows in size: the H_2–H_2 interaction becomes dominant and therefore the energy tends to a limiting value of $\sim$25 cm^{-1} (see Fig. 5) of a H_2 dimer given by our present potential choice. One should also note, however, that such value is still far from the expected bulk enthalpy value of the liquid ($\sim$52 cm^{-1} [31]) but already fairly close to that of the gas enthalpy ($\sim$23.6 cm^{-1} [31]) at the triple point.

The calculations of the lower panel in Figure 11 are also very instructive in explaining the microscopic features of the present clusters. We report there the single-H_2 evaporative energies, $\Delta E_{tot} = E_{tot}(N_{H_2}) - E_{tot}(N_{H_2} - 1)$, up to $N_{H_2} = 30$. If we take the binding energy of the lowest bound states of the $OCS(pH_2)$ complex (-77.4 cm^{-1}) and compare this value with the average evaporative energy given by the first five partners in the data of Figure 11, we find -77.5 ± 1.5 cm^{-1}, i.e. a value very well approximated by the $n = 0$ level binding energy of the single-particle VdW complex, with only a small effect from the additional $V_{H_2-H_2}$ interactions. This essential equivalence of the first five pH_2 particles in the small clusters produces, as we saw from their angular and radial density distributions, a sort of symmetric rotor structure of the complex which is thus expected to yield rotational spectra within a symmetry behaviour in agreement with the suggestion from the experimental findings [9]. The evaporative energy gets markedly reduced when going from 5 to 6 admolecules, for the reasons already discussed before.

The energies of the larger clusters from $N_{H_2} = 6$ till $N_{H_2} = 17$, are seen to remain close to the $N_{H_2} = 6$ value. From our previous discussion on the solvent spatial distributions, such clusters qualitatively correspond to adding particles to the $n = 2$ zeroth-order level located around the sulphur end but further away from the molecular axis.

One should also note that the large error bars shown by the results in the lower panel of Figure 11 do not really allow to attribute physical significance to the oscillations shown by the binding energies between $N_{H_2} = 10$ and 20. It is however clear from our results that: (i) the initial 5–6 admolecules are forming the strongest shell around the dopant and that (ii) beyond $N_{H_2} = 20$ one has essentially completed the first shell of solvation and the interaction is dominated by the H_2–H_2 potential. Since such qualitative conclusions can already be made from the present level of calculations, we did not deem necessary to push further down the energy error bars shown here.

A steady decrease of the evaporative energy is seen to occur from 18 to 30 admolecules in the cluster, while the corresponding average energy for admolecule, E_{tot}/N_{H_2}, reported in the last column of Table 2 remains largely constant up to $N_{H_2} = 20$ and shows only a slight decrease in the larger clusters. It is interesting to note that the energy values associated to single atom evaporation and to the average H_2 binding values of Table 2 are very close, for the smaller N_{H_2} clusters, with those given by reference [13] since the OCS–H_2 interaction is dominant and they use there our same potential. However, some departure

between the two set of values occurs beyond $N_{H_2} \sim 6$ since the H_2–H_2 interaction plays an increasingly more important role and our choice for it is different from that of reference [13].

5 Conclusions

We have described at the microscopic level the energetics and the structural shapes of several $OCS(pH_2)_N$ clusters, with N_{H_2} up to 30 attached partners. We have further related our findings with the existing information on such complexes from the high resolution spectroscopic data taken on them when solvated in large ^{4}He droplets [7–10] and tried to define selective pH_2 collocation areas around the dopant.

Because of the complexity of the latter scenario, we have first analysed the properties of the "free" $OCS(pH_2)_N$ complexes and further simplified our treatment of the interaction by considering the pH_2 as a spherical partner within the complex. In spite of this simplification of the real potential energy surface, the latter is probably not an unrealistic assumption as the pH_2 molecule may not be much excited in its rotational motion when within the cold cluster and in the droplet environments. Therefore, we have considered only the spherical component of the pH_2–pH_2 full interaction, a simplifying picture which is also in keeping with the previous choice. The employed OCS–(pH_2) potential energy surface was therefore taken to be that of the corresponding rigid rotor partners, leaving only two explicit Jacobi coordinates in the PES of each "monomeric" $OCS(pH_2)$ complex. It was obtained from earlier ab initio calculations that included dependence on the pH_2 relative orientations [14] and we have averaged over those orientations.

The stochastic calculations carried out for several clusters provide us with the following picture:

1. about five to six pH_2 adparticles locate themselves in energetically equivalent positions and form a sort of "doughnut" perpendicular to the dopant's molecular main axis, at about 3.7 Å from it, defining a specific region around the dopant;
2. the structure of the corresponding overall rotor therefore looks like that of a symmetric rotor that, when rotations were to be excited, should not exhibit Q branch rotational transitions, in agreement with the experimental findings [9];
3. beyond the $H_{H_2} = 6$ cluster our calculations show that the addition of the 7th particle brings it mostly on the sulphur side and pushes the 6th admolecule more clearly around the "doughnut", thereby making the cluster the shape of an asymmetric rotor: indeed the experiments show that for such clusters one detects the appearance of a Q branch in the spectrum from $N_{H_2} = 7$ [7–10];
4. the larger aggregates from $N_{H_2} = 8$ till $N_{H_2} = 17$ bring the new pH_2 molecules either chiefly on the sulphur side or on both the dopant's ends. All the larger rotors should therefore have asymmetric structures as found by the experiments [9];
5. we further see from our calculations that a simple, zeroth order description of the energetics could be had by using the structures of the bound states of the "single particle" complex, the $OCS(pH_2)$ VdW system, where geometry and moments of inertia were also found by our calculations to be in general accord with the experiments [15]. Thus, our present work suggests that the first six pH_2 particles behave like nearly independent, entirely equivalent single-complex partners occupying the $n = 0$ bound state of the one pH_2-complex so that the global wavefunction of the cluster could be described as a Hartree-type product of single-particle wavefunctions of that $n = 0$ state of the OCS–pH_2 unit system.. The simple sum of the single-particle eigenvalues produces, in fact, a total energy which differs less than 5% from the DMC total energies obtained by us.
6. while the $N_{H_2} = 6$ system still remains a nearly symmetric rotor, the next cluster, ($N_{H_2} = 7$), and those beyond up to $N_{H_2} = 25$, are all with the additional particles occupying more excited states and moving away from the central doughnut.

On the whole, the present calculations strongly suggest that the "solvation" of the OCS dopant in the pH_2 clusters gets nearly completed with the first 20 molecules and agrees reasonably well with the experiments or the OCS $(pH_2)_N$ clusters immersed in He droplets that analysed the rotating VdW complex [8–10]. In spite of the simplified interaction potentials we have adopted, therefore, our present model provides a reasonable explanation of the existing measurements and suggests that the stronger $OCS(pH_2)$ interaction prevents the He atoms from getting inside the first layer of (pH_2) partners that are therefore located more closely around OCS.

We are grateful to Dr. K. Higgins for letting us have his computed OCS–pH_2 PES and Dr. B. Whaley for many clarifying discussions on the DMC methodology of reference [30]. The financial support of the Italian Ministry for University and Research (MUIR), together with that from the Max-Planck-Society, are gratefully acknowledged. One of us (FAG) also thanks Dr. A. Vilesov and Professor J.P. Toennies for the sharing of their measurements. We further thank Dr.s C. Di Paola and E. Bodo for helping with the preparation of the figures and the referee for several helpful comments.

References

1. J.P. Toennies, A.F. Vilesov, K.B. Whaley, Phys. Today **54**, 31 (2001), and references therein
2. J.P. Toennies, A.F. Vilesov, Ann. Rev. Phys. Chem. **49**, 1 (1998)
3. J.P. Toennies, A.F. Vilesov, Angew. Chem. Int. Ed. **43**, 2622 (2004)
4. S. Grebenev, J.P. Toennies, A.F. Vilesov, Science **279**, 2083 (1998)
5. F. Paesani, F.A. Gianturco, K.B. Whaley, Europhys. Lett. **56**, 658 (2001)

6. F. Paesani, F.A. Gianturco, K.B. Whaley, J. Chem. Phys. **115**, 10225 (2001)
7. S. Grebenev, B.G. Sartakov, J.P. Toennies, A.F. Vilesov, Science. **289**, 1532 (2000)
8. S. Grebenev, B.G. Sartakov, J.P. Toennies, A.F. Vilesov, J. Chem. Phys. **114**, 617 (2001)
9. S. Grebenev, E. Lugovoi, B.G. Sartakov, J.P. Toennies, A.F. Vilesov, Faraday Discuss **118**, 19 (2001)
10. S. Grebenev, B.G. Sartakov, J.P. Toennies, A.F. Vilesov, Phys. Rev. Lett. **89**, 225301 (2002)
11. S. Grebenev, , B.G. Sartakov, J.P. Toennies, A.F. Vilesov, J. Chem. Phys. **118**, 8656 (2003)
12. Y. Kwon, K.B. Whaley, Phys. Rev. Lett. **89**, 273401 (2002)
13. F. Paesani, R.E. Zillich, K.B. Whaley, J. Chem. Phys. **119**, 11682 (2003)
14. K. Higgins, private communication
15. J. Tang, A.R.W. McKellar, J. Chem. Phys. **116**, 646 (2002)
16. R.C. Cohen, R.J. Saykally, J. Chem. Phys. **95**, 7891 (1991)
17. R.C. Cohen, R.J. Saykally, J. Chem. Phys. **98**, 6007 (1993)
18. BOUND Computed Code version n. 5. Distributed by the Collaborative Computational project n. 6 of the former SERC Council of the U.K.
19. J.A. Schaefer, Z. Phys. D **13**, 217 (1989)
20. U. Buck, F. Huisken, A. Kohlhase, D. Otten, J. Chem. Phys. **78**, 4439 (1983)
21. F. Paesani, F.A. Gianturco, M. Lewerenz, J.P. Toennies, J. Chem. Phys. **111**, 9897 (1999)
22. F. Paesani, F.A. Gianturco, M. Lewerenz, J.P. Toennies, J. Chem. Phys. **111**, 10892 (1999)
23. D.M. Ceperly, B. Adler, Science **231** 555 (1986)
24. W.A. Lester, B.L. Hammond, Ann. Rev. Phys. Chem. **41**, 283 (1990)
25. J.B. Anderson, Int. Rev. Phys. Chem. **14**, 85 (1995)
26. M. Lewerenz, R.O. Watts, Mol. Phys. **81**, 1075 (1994)
27. R.N. Barnett, P.J. Reynolds, W.A. Lester Jr, J. Comput. Phys. **96**, 258 (1991)
28. M. Lewerenz, J. Chem. Phys. **104**, 1028 (1996)
29. We thank A. Viel, K.B. Whaley for providing us with some of the routines employed in our DMC treatment, F. Paesani for the porting of them on our workstations
30. A. Viel, M. Patel, P. Niyaz, K.W. Whaley, Comp. Phys. Comm. **145**, 24 (2002)
31. E.L. Knuth, F. Schuenemann, J.P. Toennies, J. Chem. Phys. **102**, 6258 (1995)